small science
www.small-science-journal.com

Multifunctional Piezoelectric Yarns and Meshes for Efficient Fog Water Collection, Energy Harvesting, and Sensing

*Gregory Parisi, Piotr K. Szewczyk, Shankar Narayan, Daniel P. Ura, Joanna Knapczyk-Korczak, and Urszula Stachewicz**

Given global water scarcity and the quest for sustainable energy, there's a pressing need for integrated approaches addressing water-energy interdependence worldwide. A practical approach for this challenge involves the implementation of fog water collectors. Herein, a polyvinylidene fluoride (PVDF) multifunctional device capable of harvesting water and electricity from wind is developed and tested, collecting up to 365 mg cm^{-2} h^{-1} of fog water. Due to the piezoelectric nature of electrospun PVDF, these yarns and meshes not only serve as piezoelectric sensors, enabling the detection of incoming fog flow and determination of its speed and, bust also harvest electricity by charging a capacitor, making it a green and renewable power source. In this study, promising insights are offered into developing efficient fog water collection methods and utilizing piezoelectric fiber-based yarns and meshes for multifunctional applications in sustainable water management, energy harvesting, and sensing in a single device.

1. Introduction

Global water scarcity is a pressing issue that poses significant challenges for various sectors, including agriculture, industry, and domestic water supply, jeopardizing sustainable development and human well-being.[1] Sustainable methods of solving this issue include implementing solar evaporation for drinking water,[2] advancing solar farming with minimal environmental impact,[3] and promoting vapor-harvesting techniques to capture atmospheric moisture.[4] Fog water collection is a technique that involves collecting water droplets from the air.[5] This method is particularly useful in areas where traditional water sources are scarce or inaccessible, such as coastal regions, mountainous areas, or cloud forests.[6] Collecting water from fog involves using specialized structures made of nets, meshes, or harps.[7] Fog-collecting nets are typically made of specially designed mesh material that allows air to pass through while collecting water droplets.[8] Fog harps or yarns comprise an array of fine, vertically oriented wires that bypass clogging issues typically found in meshes and nets.[9] As tiny water droplets build up on the net, they form larger droplets, which flow down into a collection system under gravity.

To create highly porous fibrous meshes, which are permeable, electrospinning is often used[10] and randomly deposited fibers can be applied for fog water collection.[11] Additionally, electrospinning can be used to tailor the piezoelectricity and functional properties of the fibers, such as the surface[12] and mechanical properties.[13] In contrast to nets, nanofiber meshes are tunable with precise control over fiber diameter, morphology, and wetting properties.[14] Among the prominent piezoelectric polymers,[15] polyvinylidene fluoride (PVDF) stands out as a key candidate,[16] extensively employed in the creation of smart textiles[17] and medical applications.[18] In addition to meshes, the development of yarns is ongoing.[19]

In recent years, there has been an increasing interest in improving the design and efficiency of fog collectors to enhance water collection rates (WCRs). Inspired by nature, various materials and techniques have been developed to mimic the Namib Desert Beetle[20] or the spine of the cactus.[21] Numerous approaches have been conducted with different mesh materials,[22] surface coatings,[23] and collector shapes[24] to optimize water droplet collection and minimize water loss. One method involves changing the wettability of the fibers on a fog collector to take advantage of both the hydrophobic and hydrophilic properties.[25] Wettability alteration on smart surfaces occurs in nature and has also been successfully implemented in various applications, such as droplet manipulation,[26] switchable surfaces,[27] oil–water separation,[28] liquid transport,[29] and thermal management.[30] Thakur et al.[31] showed that switchable

G. Parisi, S. Narayan
Department of Mechanical, Aerospace, and Nuclear Engineering
Rensselaer Polytechnic Institute
110 8th Street, Troy, NY 12180, USA

P. K. Szewczyk, D. P. Ura, J. Knapczyk-Korczak, U. Stachewicz
Faculty of Metals Engineering and Industrial Computer Science
AGH University of Krakow
al. A. Mickiewicza 30, 30-059 Krakow, Poland
E-mail: ustachew@agh.edu.pl

The ORCID identification number(s) for the author(s) of this article can be found under https://doi.org/10.1002/smsc.202400021.

DOI: 10.1002/smsc.202400021

wettability for electrospun fibers could be used for water-harvesting applications. They employed a thermoresponsive polymer to assess WCRs under varying temperature conditions. Additionally, Lalia et al.[32] impregnated electrospun nanomats with lubricant to change the contact angle hysteresis and improve the water collection. Another approach to improve fog collectors involves using fog harps, which reduce the pinning force of captured droplets, facilitate quicker shedding, and prevent clogging.[33] Kowalski et al.[34] investigated different fog harps' wettability to optimize key parameter combinations. Interestingly, the enhanced water-harvesting efficiency of fog collectors was noticed by incorporating electrospun aligned fibers into commercially available meshes.[11] However, so far, there is no research combining the piezoresponse of materials and fog water collection to design all-in-one setup harvesting water and energy. Smart materials, particularly piezoelectric nanogenerators, have gained prominence in energy harvesting, capitalizing on their unique ability to exhibit multifunctional properties in response to external stimuli, which extends beyond their primary functions, making them highly versatile across various applications. For example, superhydrophobic surfaces, an example of hydrophobic smart materials, are being investigated for their potential in enhancing energy-harvesting capabilities by improving droplet mobility and condensation processes.[35] The field of water purification has explored multifunctional smart materials by integrating graphene oxide and MXenes in 3D structures to enhance contaminant adsorption and incorporating catalytic sites or antimicrobial agents within the purification system.[36]

Nature is an inspiration, drawing insights from phenomena like spiderwebs[37] and redwoods[38] for researchers. This interest in nature-inspired materials has led to the exploration of multifunctional properties in different applications.[39] Piezoelectric polymers hold significant importance in materials engineering and unlike traditional piezoelectric materials like ceramic are flexible and lightweight. This makes construction for fog harvesters easier, portable, and adaptable to different shapes. To further enhance the use of fog collectors, we fabricated a highly efficient fog collector by electrospinning piezoelectric PVDF yarns to form harps. The produced yarns are a multifunctional part of water collection capabilities, serving as a wind-sensing station and energy-harvesting material. Here, we demonstrate for the first time a one-step process to obtain fog-harvesting piezoelectric yarns capable of generating power and harvesting water from the air to secure a greener and water-resilient future, as presented schematically in **Figure 1**.

2. Results and Discussion

2.1. System Design—Morphology and Wettability

Water-harvesting systems constructed from electrospun PVDF fibers excel in multifunctionality and efficiently collect water from foggy air, detect approaching fog, measure wind speed, and generate electricity. The electrospun collector is lightweight and shape-adjustable. Therefore, the uniformity and structure of electrospun PVDF yarns are of paramount importance in this study, given their influence on material performance and functionality. Notably, these morphological aspects are closely linked to the hydrophobic nature of the materials, which is key to facilitate more rapid droplet removal from yarns as compared to meshes. The macroscale geometry of the PVDF yarns contribute significantly to their durability and efficiency in water capture. The scanning electron microscope (SEM) analysis of PVDF electrospun yarns and meshes is depicted in **Figure 2**a–d. In both yarns and meshes, PVDF fibers exhibit uniformity, continuity, and a lack of bead formations. The average fiber diameter measures at $2.3 \pm 0.6\,\mu m$ for yarns and $2.2 \pm 0.4\,\mu m$ for meshes, Figure 2e. While these materials share similarities in morphology and fiber diameter, the pivotal influence on macroscale geometry resides in the manufacturing process. The mesh presents a relatively flat surface at the macroscale, while PVDF yarns undergo individual bundling to construct an efficient water-capturing surface, Figure 2. Notably, the average diameter of the PVDF yarn measures $352 \pm 19\,\mu m$ (Figure S1, Supporting Information). For comprehensive insights into the chemical composition, additional Fourier transform infrared (FTIR) spectroscopy characterizations of both yarns and meshes are present (Figure S2, Supporting Information). Regarding the tensile testing and durability assessments, it was conducted previously indicating the enhanced mechanical strength of electrospun PVDF meshes due to their high surface-area-to-volume

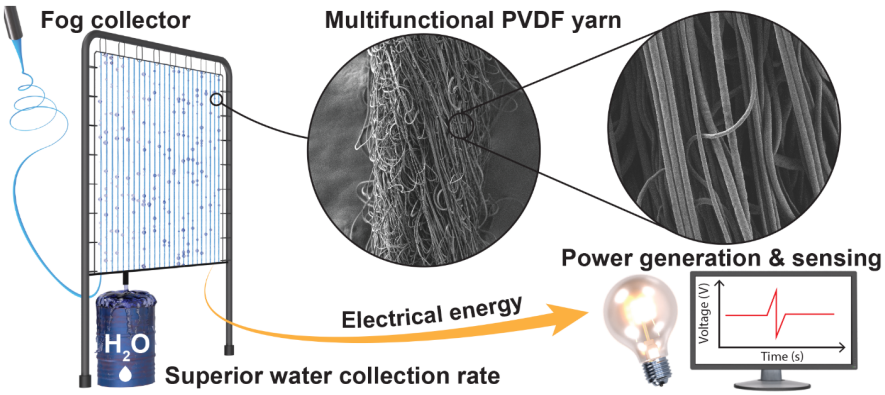

Figure 1. Design of fog collector using electrospun fibers to form yarns used as a harp system with multifunctional capabilities in harvesting water and energy.

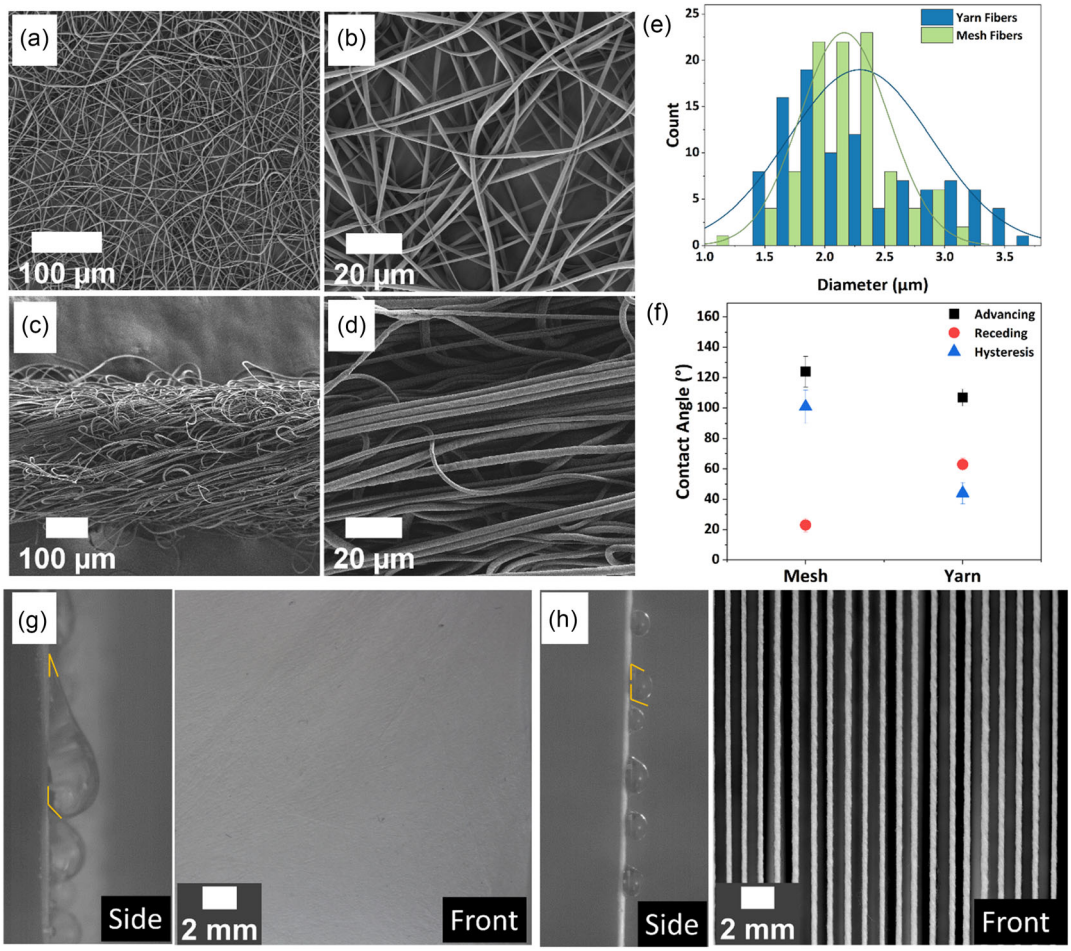

Figure 2. The SEM micrographs of a,b) PVDF mesh, c,d) PVDF yarn, and e) PVDF fiber diameter distribution in f) meshes and yarns. Dynamic contact angle of the mesh and yarn g) optical images of water droplet contact angle hysteresis on PVDF mesh h) optical images of water droplet contact angle hysteresis on PVDF yarns.

ratio and inherent flexibility.[11] Long-term stability studies of PVDF piezoelectric generators under a cyclic load have also already been performed, revealing exceptional stability.[40] Fabricating synthetic fibers with the extra support of yarn can show superior mechanical properties of tensile strength and toughness.[41] Additionally, PVDF yarns fabricated via electrospinning demonstrate long-term durability and resilience and can withstand many mechanical impact cycles.[42] The feasibility of fabricating stretchable fibers for water and energy harvesting has been also demonstrated previously[43] and manifests the potential of electrospinning to yield stretchable fibers suitable for water-harvesting applications.[44]

The wetting behavior of PVDF meshes and PVDF yarns, despite their shared polymer and similar fiber diameters,[45] exhibits significant distinctions due to their macroscopic geometry. Figure 2f illustrates the advancing and receding contact angles along with the contact angle hysteresis. A high contact angle hysteresis, approaching 90°, results in droplets adhering to the sample and growing on the collector until a critical volume is reached, causing them to roll off. Conversely, materials with lower contact angle hysteresis, like PVDF yarns, facilitate quicker droplet roll-off, as they exhibit weaker adhesion to the surface.[46] In Figure 2g, the PVDF mesh's random fiber alignment retains shedding droplets on its surface, requiring a larger droplet size for gravity to initiate detachment into the collection reservoir. In contrast, Figure 2h portrays the behavior of droplets on PVDF yarns designed for fog water collection. Despite sharing the same surface chemistry, their distinct geometries result in remarkably different interactions with fog water droplets. The PVDF yarns allow unobstructed droplet sliding into the reservoir, minimizing hindrances caused by horizontal yarns and random fiber alignment.[47] Electrospun meshes typically have a high porosity and the randomly connected fibers forming an open network. This structure often results in a large surface area which can promote greater interaction between the water droplets and the surface of fibers. As a result, electrospun meshes can exhibit a higher contact angle hysteresis, indicating better wetting and enhanced water adhesion. In contrast, electrospun yarns are more compact and have a lower porosity due to aligned and twisted fibers. This aligned structure can result in a reduced surface area and lower roughness than meshes. Consequently, the contact angle hysteresis on electrospun yarns can be lower, indicating less favorable

wettability and reduced water adhesion compared to meshes. Additionally, the reduced surface area of the yarns' limits droplet adhesion, further enhancing droplet shedding and collection efficiency. These observations are closely tied to the lower contact angle hysteresis exhibited by the yarns, as shown in Figure 2f.

2.2. Fog Water Collection

The WCR results, **Figure 3**a,b, indicate that PVDF yarns collected 104% more water than mesh. Within the first 15 min of the experimental fog capture, the PVDF yarns had a collection rate seven times higher than the PVDF mesh, 213 and 29 mg cm^{-2} h^{-1}, respectively. After 3 h, steady-state WCRs of 365 mg cm^{-2} h^{-1} for the PVDF yarns and 115 mg cm^{-2} h^{-1} for the PVDF mesh were achieved. Water retained on a fog water collector decreases the collection efficiency, and the optimized yarns quickly shed droplets instead of retaining the droplets. The fog water collection on Raschel mesh was also measured, approximately 217 mg cm^{-2} h^{-1} after 3 h, as a comparison (Figure S3, Supporting Information), because it is one of the most common methods employed for fog water collection. Previously, it has been shown that adding hydrophilic nanofibers reduces the retained water and improves the WCR from 16 to 60 mg cm^{-2} h^{-1}.[48] Yin et al.[49] also increased water collection by incorporating micro/nanopatterns to achieve a WCR of 200 mg cm^{-2} h^{-1}. Fog water harvesting is influenced by humidity conditions,[50] which is beyond the focus of this study. Higher humidity levels facilitate more efficient fog capturing capabilities due to the increased availability of water vapor for condensation.[51] The indoor tests for fog water collection should be always performed in at a maximum 100% humidity.[37]

The droplet dynamics were quantitatively measured using high-speed visualization (Video S1, Supporting Information). Droplet speed was deduced by measuring the change in droplet position with time Figure 3c. The single yarns had the fastest average velocity, 180 mm s^{-1}, compared to the yarns array and mesh, 154 and 123 mm s^{-1}, respectively. The time it takes for a droplet to shed, replenish, and then shed again was also calculated (Figure 3d). The single yarns shed droplets over 70 times quicker than the mesh, and introducing multiple yarns to create a yarns array only slightly decreased the shedding rate from 63 to 51 drops min^{-1} cm^{-2}. For droplet shedding, the critical volume also plays an essential role in how fast droplets are evacuated to a collection reservoir (Figure 3d). To facilitate droplet rolling off the mesh, a critical volume of ≈12.2 µL, on average, is required. In contrast, the PVDF yarns exhibit significantly smaller average critical volumes, with 1.4 µL for individual yarns and 3.6 µL for the yarns array. The yarn geometry of electrospun PVDF can significantly enhance the fog water collection efficiency. Wu et al.[52] also used a directional surface for improving water collection and obtained a WCR of 30 mg cm^{-2} h^{-1} on plasma-etched silicon water. Joon Lee et al.[21] used a double-structural hydrogel system

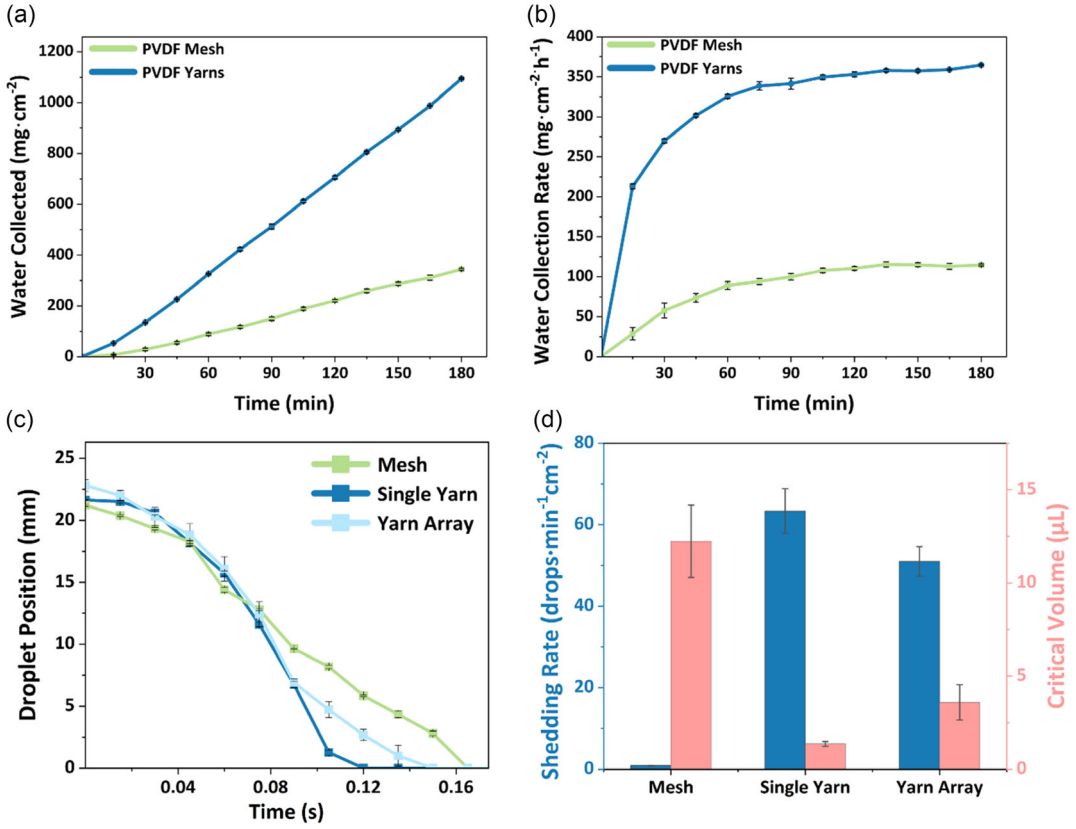

Figure 3. The results of a) water collection of the PVDF mesh versus the PVDF yarns and b) water collection rate of PVDF mesh versus c) the PVDF yarn position of a water droplet sliding down the surface. d) Plots showcasing the comparison between PVDF mesh, PVDF single yarn, and PVDF yarns array. The water droplet shedding rate (blue) and the critical volume of a sliding water droplet (pink).

to improve directional water transport and obtained a WCR of 209 mg cm^{-2} h^{-1}. Creating electrospun meshes for fog water collection improves the surface area while maintaining high permeability, which is why researchers have studied electrospun meshes over commercially available nets.[53] More recently, it was found that harps had an improved WCR compared to meshes.[54] Thus, the enhanced water collection using electrospun PVDF can be attributed to the droplet dynamics by changing the geometry from a mesh to a yarn. The PVDF mesh can capture fog droplets from the air due to its high permeability and large surface area. Here, the high-speed imaging, presented in **Figure 4**, was used to capture the droplet shedding during the fog water harvesting (Video S1, Supporting Information). Due to gravity, the large droplet fell down the mesh and gathered smaller droplets of water that were directly beneath it. In comparison, much smaller droplets are shed from the PVDF yarn.

Yarns provide more efficient water harvesting due to their ability to support faster droplet movement and detachment, as they possess less direct contact surface area to water droplets compared to the mesh. The gravitational force must exceed an adhered droplet's surface tension to detach from the surface.[55] The faster droplet shedding dynamics and enhanced detachment from the yarn's structure contribute to its superior water-harvesting efficiency compared to mesh. In the case of the

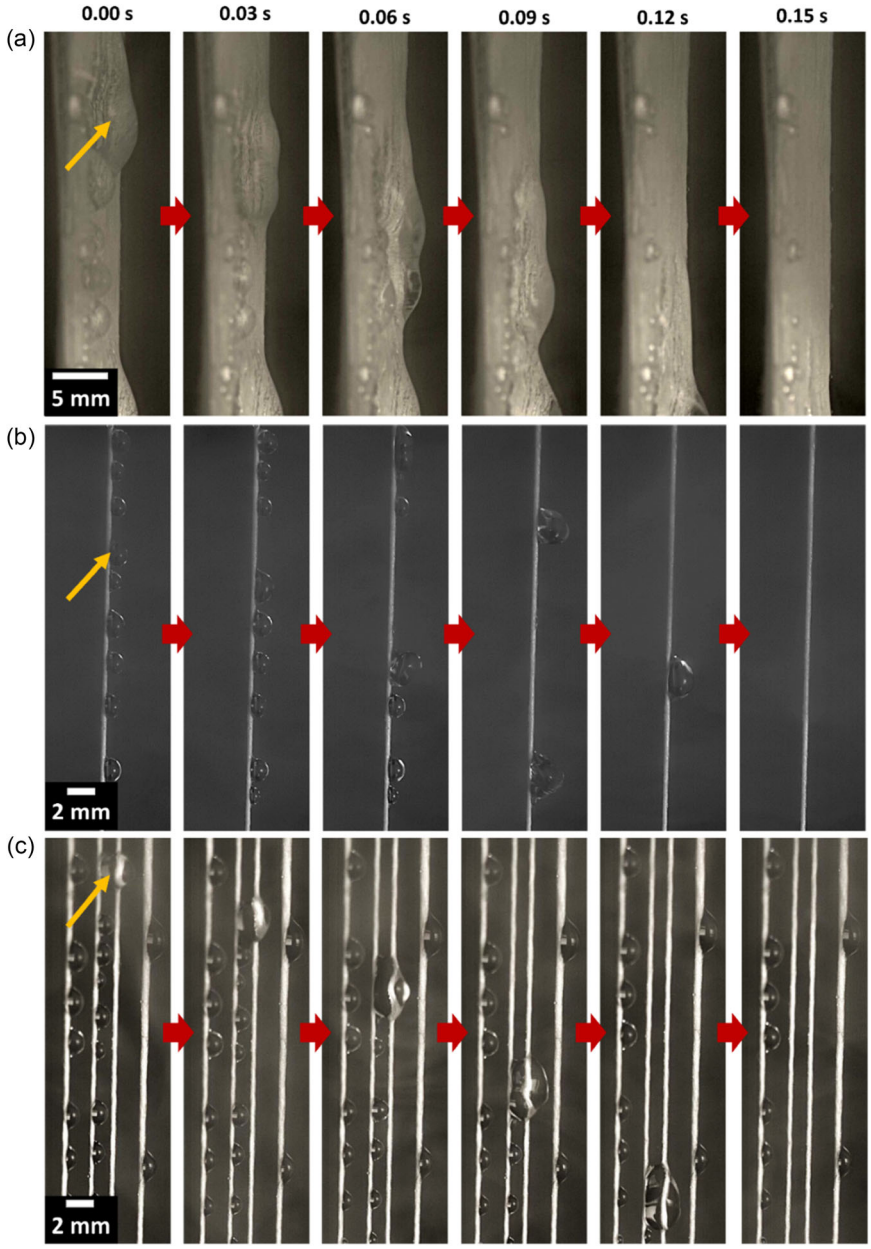

Figure 4. Time-lapse of droplet sliding down on a) PVDF mesh, b) a single PVDF yarn, and c) a PVDF yarn array. The yellow arrow indicates the droplet initially beginning to shed, and the time stamp relates to all columns.

PVDF mesh, Figure 4a, there is a higher surface area in contact with the droplet compared to the PVDF yarn. A water droplet can move freely down the yarns, contributing to a faster droplet speed than the mesh. Figure 4b shows that a droplet of water moves down the yarns quicker than a droplet of water moves down the mesh. The droplet on the mesh was evacuated entirely within 0.15 s; however, two droplet events occurred within 0.15 s on the yarn. The PVDF electrospun yarns had an initial droplet shed on the surface and collected six additional droplets below it, while a second drop above initiated the shedding process and collected three additional droplets. The enhanced water contact angle hysteresis of the PVDF electrospun yarns also influences how quickly the droplets roll down the surface of the yarn. A yarn array was studied for a more relatable comparison to see how the droplet dynamics change with multiple yarns. Figure 4c shows that a single droplet creates a liquid bridge between two adjacent yarns and still slides down the yarn array within 0.15 s. The morphological transition of a liquid placed between two fibers depends on both the system's macroscale geometry and the liquid's volume.[56] In most cases, the droplet shed also collects additional droplets below it and occasionally collects droplets on neighboring yarns.

Another factor that influences the efficiency of fog water harvesting is the environmental temperature, affecting the rate of condensation and the saturation vapor pressure of water in the air.[57] Higher temperatures generally lead to faster evaporation and lower relative humidity (RH), potentially reducing fog density and, consequently, harvesting efficiency. Conversely, lower temperatures favor a condensation process that can additionally occur and higher RH, increasing the potential for water collection.[58] By monitoring environmental temperature in real-time, the harvesting mechanisms to optimize fog water collection efficiency can be adjusted.

2.3. Energy Harvesting

The piezoelectric capabilities of PVDF meshes and yarns make them highly promising candidates for various applications, particularly in energy harvesting and sensing. Their demonstrated capacity to generate electricity from mechanical stress underscores their role in state-of-the-art fog collection and weather-monitoring facilities. The piezoelectric effect of the PVDF meshes and PVDF yarns was measured to show the multi-application potential in energy harvesting and sensing. The average d_{33} piezoelectric coefficient (pCN) for the PVDF meshes and PVDF yarns, 7.8 ± 0.7 and 8.4 ± 0.5 pCN, respectively. This measurement shows that both fog collectors can generate electricity from the transformation of mechanical stress—something that would constantly happen in windy conditions during the outside use of a large-scale fog collector. Additionally, the PVDF yarns and meshes can be used as a fog sensor or a generator to power a weather station powered by the piezoelectric properties of the material itself.[59]

Within this study, we also tested the possibility of sensing changes in air movement, where the meshes and yarns were exposed to air streams of different velocities. In **Figure 5**a, the schematic of piezoelectric charging and sensing setup is shown. The wind speeds used in the study[60] closely resemble typical everyday wind speeds found in outdoor settings and are also typical for other wireless weather stations in mountain areas,[61] varying between a gentle breeze and a strong breeze (15–45 km h^{-1}). As shown in Figure 5b, the electrospun materials respond to different air streams with a voltage of 371 ± 85 and 11.6 ± 5.6 mV at the lowest fog speed for the meshes and yarns, respectively. At the highest fog speed, the voltage output of the meshes was 1127 ± 309 and yarns 100 ± 34 mV, respectively. Full statistical descriptions of the outputs of the meshes and yarns are also present in Table S1, Supporting Information. The piezoelectric setup used can be found in detail in Figure S4, Supporting Information. This sensor could be used as an indicator in fog water collection if the mesh is in contact with fog at certain points of the day. Further, a capacitor charging test was carried out to verify the possibility of powering small electronics. A perpendicular, cyclic stream of air at different speeds was introduced at a frequency of 2 Hz to both PVDF meshes and PVDF yarns. Figure 5c demonstrates that the mesh can charge a capacitor to a stable level of 5.0 V, while Figure 5d illustrates that the yarns are capable of charging a capacitor to a stable level of 1.1 V. Other groups have shown the charging of a capacitor to 0.8 V with piezoelectric material using a 683 nF capacitor.[62]

The measured piezoelectric effect of the PVDF meshes and PVDF yarns highlights their versatile potential for energy harvesting and sensing applications. Both types of fog collectors demonstrated the ability to generate electricity from mechanical stress, making them suitable for a state-of-the-art fog-collecting and weather-monitoring facility. In Figure 5c,d, we show the capacitance charging from the mechanical stress of the PVDF, showcasing the potential to generate sustainable energy from such a device. The experimental results demonstrated the capability of charging capacitors to steady voltage levels, confirming the materials' responsiveness to different air stream velocities. Our results build upon previous research examining load matching, current output, and mechanical stability.[42] In that work, the PVDF yarn displayed significant responsiveness, yielding a maximum root-mean-square (RMS) power output of 72 nW at a 400M Ω resistance. Additionally, the open-circuit voltage (V_{oc}) measured 2.6 V, and the short-circuit current (I_{sc}) was 465 nA. As for meshes in a previous study, the same material was able to achieve a maximum average output of 0.58 μW at 100 MΩ, under 20 N load and 1 Hz frequency.[40]

The piezoelectric effect in PVDF and similar materials has been well documented in scientific literature. These materials generate electrical charges and can enhance the efficiency of water harvesting. As fog droplets come into contact with the PVDF collector, they impart mechanical energy to the materials and induce electric charges within the PVDF. These charges, in turn, can affect the behavior of the water droplet on the surface.[63] The mobility of the droplets are affected by the charge and can influence the WCR in which smaller water droplets roll off without the need for excessive droplet coalescence.[64] In summary, we show that PVDF yarns maximize water collection efficiency, and the PVDF meshes provide higher energy output. The current results are compared with competing materials used in water harvesting and piezoelectric energy generation Figure 5e. However, this is the first study that has multifunctional superior properties of water and energy generation showed on harp system from yarns. The piezoelectric performance can be increased and designed to work with triboelectric nanogenerator approach

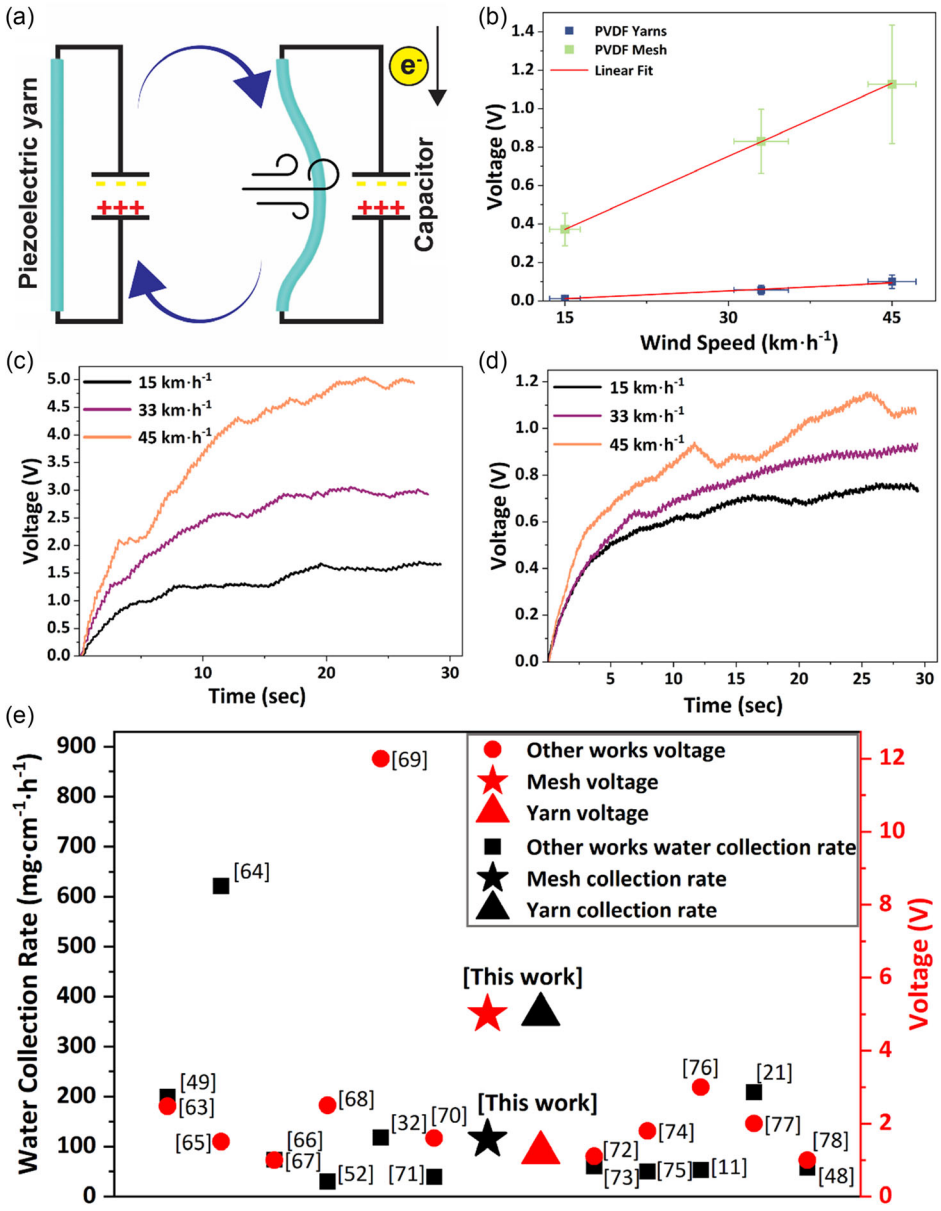

Figure 5. a) Piezoelectric charging and sensing schematic setup. b) Sensing capabilities at different wind speeds of meshes and yarns. c) Charging of a 10 μF capacitor using PVDF meshes and d) PVDF yarns. e) Summary of fog water collection rate and capacitor charging of different materials from the following:[11,21,32,48,49,52,65–80] red circle indicates other works voltage, black square indicates other works water collection rate, the red star indicates this works voltage, and the black star indicates this works water collection rate.

in the future for much higher energy outputs. The multifunctionality of electrospun fibers is exemplified using PVDF yarns and mesh configurations, highlighting the diverse potential impact of such materials in varying geometrical arrangements. This hybrid approach offers a unique optimization of resource utilization. Beyond its primary function of water collection, the surplus energy harvested can be effectively harnessed to power humidity sensors, lighting systems, and wind sensors. Embracing a device with multiple functions presents a promising path toward a more sustainable and efficient approach to fog water collection.

3. Conclusion

Within this research, we bridge the gap between water harvesting and energy harvesting showcasing the usability of PVDF yarns and meshes. Our innovative water collector operates without the need for external power sources, making it a cost-effective and environmentally friendly solution. Here, PVDF yarns have proven to outperform meshes, achieving a fog WCR of 365 mg cm^{-2} h^{-1}, compared to 115 mg cm^{-2} h^{-1} for meshes. This superior performance can be attributed to the unhindered movement of droplets along the yarns, facilitating faster and

more efficient fog water collection. Moreover, the electrospinning process allows for the customization of fiber and yarn surface properties, providing further control over the performance and application of these materials. Our device can serve as an environmental monitor in remote locations, as PVDF meshes can autonomously charge without external energy input. Leveraging the piezoelectric effect in PVDF through electrospinning opens possibilities such as including the development of fog water sensors capable of monitoring varying wind speeds. Electrospun yarns represent a promising technology with a wide range of potential applications in fog water collection and sensing.

We bridge the gap between water harvesting and energy harvesting by showcasing PVDF yarns and meshes. The novel water collector requires no external power sources, making it highly cost-effective and environmentally friendly, if used for a weather station with energy harvesting and sensing capabilities. Moreover, this device can be used as an environmental monitor in remote locations since the PVDF meshes can charge a capacitor, with no outside energy input, to 5 V, and the PVDF yarns can do the same to a charge of 1.1 V. Utilizing the piezoelectric effect in PVDF through nanofibers opens up new possibilities, such as developing fog water sensors that can operate at different wind speeds, making electrospun yarns a promising technology with many potential applications in fog water collection and sensing.

4. Experimental Section

Materials and Solution Preparation: For the electrospinning solution, a 24 wt% solution of PVDF (Sigma-Aldrich, UK, $M_w = 350\,000$ g mol^{-1}) was dissolved in dimethylacetamide (DMAc, Sigma-Aldrich, UK), and acetone (Sigma-Aldrich, UK) in a 1:1 ratio. The solution was stirred at 400 rpm for 4.0 h on a hot plate set to 50 °C (IKA RCT basic, Staufen, Germany).

Electrospinning: The fibers were electrospun using TechNOVA (ESVY-100, MicroNano Tools, Canada) electrospinner with a climate control system. The PVDF fiber meshes were produced by applying a voltage of +18 kV to the 20 G stainless needle, which was set to 20 cm distance from the collector. The chamber's environmental conditions were kept at $T = 24$ °C and RH of 45%. The flow rate was set to 1.0 mL h^{-1}. The collector held at a constant rotating speed of 30 rpm. The PVDF fiber yarns were produced by applying a voltage of +7 kV to one 19 G stainless needle and a voltage of −8 kV to the other 19 G stainless needle, which were set to 16 cm distance from the collector. The chamber's environmental conditions were kept at $T = 25$ °C and RH of 40%. The flow rates for both pumps were set to 4.5 mL h^{-1}. The collecting mandrel was held at a constant rotating speed of 12 rpm, and the vortex speed was held constant at 350 rpm. Figure S5, Supporting Information, shows a schematic of the electrospinning process and the images of the yarns production.

Characterization: The electrospun samples were analyzed using an SEM (Merlin Gemini II, ZEISS, Germany). Prior to SEM imaging, the samples were coated with an 8 nm Au layer using a rotary pump sputter coater (Q150RS, Quorum Technologies, UK). Fiber and yarn diameters were measured from SEM micrographs using ImageJ software (1.53 k, NIH, USA). The average fiber diameter values were calculated from 100 measurements, and the error was based on the standard deviation calculated using software (2022, OriginLab, USA). The chemical composition of the fibers was analyzed using FTIR spectroscopy (Nicolet, iS-5, USA). The contact angle hysteresis was measured during fog water collection and imaged with a macrolens (EOS 700D, EF-s 60 mm, Canon, Japan). Contact angles were measured using a contact angle plug-in on ImageJ software (1.53, NIH, USA). The advancing angle was the maximum angle at which a droplet spread on the surface, while receding angle was the minimum angle at which a droplet started to contract. Hysteresis represented the difference between the advancing and receding angles and indicated the degree of irreversibility in the wetting behavior of a surface. All measurements of contact angle hysteresis were captured at the moment the water droplet began to shed off the mesh or yarn. High-speed imaging was conducted during fog water collection (3381 fps and 400 × 1000 pixels, Chronos CR14-1.0, Krontech, Canada). The sliding droplet's center-of-mass position was tracked using ImageJ analysis and analyzed in OriginLab (2022, OriginLab, USA).

Water-Harvesting Experimental Setup: The electrospun samples were placed in a large, sealed environmental chamber (50 × 60 × 40 cm) (Figure S6a, Supporting Information). The environmental chamber was held constant at a temperature of 22 ± 1 °C and a humidity of 97% ± 2% in the fog flow. The continuous fog flow is generated by a humidifier (Setti, AH900, Poland) at a flow rate of 300 mL h^{-1} and a speed of 1.4 m s^{-1}. The mesh was attached to two steel stands and placed 7 cm away from the humidifier vertically. The area of the collecting samples was constant (10 × 10 cm). A flowmeter (SOLE Uni-T, China) was used to measure the fog flow rate. The yarns were set up in the same conditions but were attached to 3D-printed in-house holders. Two holders were set 10 cm apart and finely tuned using adjustable nuts on a threaded rod. The teeth on the 3D printed holders were spaced 1.05 mm apart and had a total length of 15 cm. Fog water collection was performed in the in-house build environmental chamber and performed three times on both the electrospun PVDF mesh and electrospun PVDF yarn. The collected water was measured every 15 min for 3 h. The collected water was fed outside the chamber through a tube and collected on a balance, which was weighed at 15 min intervals. A schematic of the holders and setup for the yarns is shown in Figure S6b, Supporting Information. The WCR was calculated using

$$\mathrm{WCR} = \frac{m}{At} \tag{1}$$

where m is the mass, A is the fog collection area on the mesh or yarn, and t is the collection time.

Piezoelectric Study: The piezoelectric coefficients were measured in triplicate with a d_{33} meter (YE2730A d_{33} meter, Sinocera, China). The piezoelectric response sensor tests were carried out by placing PVDF meshes, or yarns, onto an acrylic holder with an electrode connected to both ends of the sample, Figure S4a, Supporting Information. An airstream with a known wind velocity was supplied perpendicular to the PVDF samples to generate the piezoelectric response. The output was measured using a DMM6500 Kiethley multimeter (USA). The produced peaks, along with the d_{33} measurements, are presented in Figure S7, Supporting Information. A control and reference standard were also measured to ensure the accuracy of the instrument being used (Figure S8, Supporting Information). Different wind speeds were used to show the sensitivity of the sensor. The wind speeds used range from a gentle breeze to a strong breeze to mimic common outdoor wind conditions.

To investigate energy-harvesting capabilities a, bespoke setup was constructed to charge a 10 μF capacitor using only PVDF meshes or yarns. The capacitor was connected according to Figure S6, Supporting Information. In this test, an airstream was introduced perpendicular to the PVDF samples for approximately 30 s to get a consistent charge at different wind speeds. A cyclic stream of air (2 Hz) was introduced to either the PVDF meshes with an active working area of 27 cm^2 or the PVDF yarns with 13.5 cm^2.

Supporting Information

Supporting Information is available from the Wiley Online Library or from the author.

Acknowledgements

This study was conducted as part of the BioCom4SavEn project funded by the European Research Council under the European Union's Horizon 2020

Framework Program for Research and Innovation (ERC grant agreement no. 948840). G.P. gratefully acknowledges financial support for this publication by the Fulbright U.S. Student Program, which is sponsored by the U.S. Department of State and the Polish–U.S. Fulbright Commission. Its contents are solely the responsibility of the author and do not necessarily represent the official views of the Fulbright Program, the Government of the United States, or the Polish–U.S. Fulbright Commission.

Conflict of Interest

The authors declare no conflict of interest.

Author Contributions

Conceptualization, U.S. and G.P.; methodology, G.P. and P.K.S.,; validation, G.P., P.K.S., D.P.U., J.K.K., and U.S.; formal analysis, G.P. and P.K.S.; investigation, G.P., P.K.S., and D.P.U.; resources, U.S.; data curation, G.P. and P.K.S.; writing – original draft, G.P. and U.S.; writing – review and editing, P.K.S., D.P.U., J.K.K, S.N, and U.S.; visualization, G.P.; supervision, U.S. and S.N.; project administration, U.S.; funding acquisition, G.P., S.N. and U.S. All authors have read and agreed to the published version of the manuscript.

Data Availability Statement

The data that support the findings of this study are available from the corresponding author upon reasonable request.

Keywords

energies, fibers, fog collections, polyvinylidene fluoride (PVDF), sensings, water harvestings, wettabilities

Received: January 19, 2024
Revised: March 13, 2024
Published online:

[1] M. Gigliotti, G. Schmidt-Traub, S. Bastianoni, *Encycl. Ecol.* **2019**, *4*, 426.
[2] Z. Wei, J. Wang, S. Guo, S. C. Tan, *Nano Res. Energy* **2022**, *1*, 9120014.
[3] S. Guo, Y. Zhang, H. Qu, M. Li, S. Zhang, J. Yang, X. Zhang, S. C. Tan, *EcoMat* **2022**, *4*, e12179.
[4] S. Guo, Y. Zhang, S. C. Tan, *Device* **2023**, *1*, 100099.
[5] O. Klemm, R. S. Schemenauer, A. Lummerich, P. Cereceda, V. Marzol, D. Corell, J. Van Heerden, D. Reinhard, T. Gherezghiher, J. Olivier, P. Osses, J. Sarsour, E. Frost, M. J. Estrela, J. A. Valiente, G. M. Fessehaye, *Ambio* **2012**, *41*, 221.
[6] J. O. Juvik, D. Nullet, *J. Appl. Meteorol.* **1995**, *34*, 2108.
[7] D. M. Fernandez, A. Torregrosa, P. S. Weiss-Penzias, B. J. Zhang, D. Sorensen, R. E. Cohen, G. H. McKinley, J. Kleingartner, A. Oliphant, M. Bowman, *Aerosol Air Qual. Res.* **2018**, *18*, 270.
[8] J. K. Domen, W. T. Stringfellow, M. K. Camarillo, S. Gulati, *Clean Technol. Environ. Policy* **2014**, *16*, 235.
[9] W. Shi, L. H. De Koninck, B. J. Hart, N. G. Kowalski, A. P. Fugaro, T. W. Van Der Sloot, R. S. Ott, B. S. Kennedy, J. B. Boreyko, *ACS Appl. Mater. Interfaces* **2020**, *12*, 48124.
[10] Z. J. Krysiak, Ł. Kaniuk, S. Metwally, P. K. Szewczyk, E. A. Sroczyk, P. Peer, P. Lisiecka-Graca, R. J. Bailey, E. Bilotti, U. Stachewicz, *ACS Appl. Bio Mater.* **2020**, *3*, 7666.
[11] J. Knapczyk-Korczak, P. K. Szewczyk, D. P. Ura, R. J. Bailey, E. Bilotti, U. Stachewicz, *Sustain. Mater. Technol.* **2020**, *25*, e00191.
[12] D. P. Ura, J. Knapczyk-Korczak, P. K. Szewczyk, E. A. Sroczyk, T. Busolo, M. M. Marzec, A. Bernasik, S. Kar-Narayan, U. Stachewicz, *ACS Nano* **2021**, *15*, 8848.
[13] M. Polak, K. Berniak, P. K. Szewczyk, J. E. Karbowniczek, M. M. Marzec, U. Stachewicz, *Appl. Surf. Sci.* **2023**, *621*, 156835.
[14] V. A. Ganesh, A. S. Ranganath, A. Baji, H. K. Raut, R. Sahay, S. Ramakrishna, *Macromol. Mater. Eng.* **2017**, *302*, 1600387.
[15] M. Smith, S. Kar-Narayan, *Int. Mater. Rev.* **2022**, *67*, 65.
[16] M. Zhang, C. Liu, B. Li, Y. Shen, H. Wang, K. Ji, X. Mao, L. Wei, R. Sun, F. Zhou, *Nanoscale Adv.* **2023**, *5*, 1043.
[17] G. Priniotakis, U. Stachewicz, J. van Hoof, *Indoor Built Environ.* **2022**, *31*, 1443.
[18] A. Ivanoska-Dacikj, U. Stachewicz, *Rev. Adv. Mater. Sci.* **2020**, *59*, 487.
[19] D. Kim, Z. Yang, J. Cho, D. Park, D. H. Kim, J. Lee, S. Ryu, S. W. Kim, M. Kim, *EcoMat* **2023**, *5*, 1.
[20] F. Guo, Z. Guo, *RSC Adv.* **2016**, *6*, 36623.
[21] S. J. Lee, N. Ha, H. Kim, *ACS Sustain. Chem. Eng.* **2019**, *7*, 10561.
[22] G. Huang, H. Xu, Y. Jin, L. Huo, J. Zhao, Z. Li, *Mater. Lett.* **2021**, *289*, 129424.
[23] Y. Wang, L. Zhang, J. Wu, M. N. Hedhili, P. Wang, *J. Mater. Chem. A* **2015**, *3*, 18963.
[24] Y. Jiang, C. Machado, K. C. K. Park, *Droplet* **2023**, *2*, e55.
[25] J. Knapczyk-Korczak, D. P. Ura, M. Gajek, M. M. Marzec, K. Berent, A. Bernasik, J. P. Chiverton, U. Stachewicz, *ACS Appl. Mater. Interfaces* **2020**, *12*, 1665.
[26] X. Liang, D. Li, S. Li, C. Xu, Z. Guo, *Langmuir* **2021**, *37*, 5745.
[27] G. Parisi, S. Narayan, *Chem. Eng. Process. – Process Intensif.* **2022**, *181*, 109165.
[28] G. Parisi, S. Narayan, *J. Water Process Eng.* **2021**, *44*, 102365.
[29] X. Wang, J. Zeng, J. Li, X. Yu, Z. Wang, Y. Zhang, *J. Mater. Chem. A* **2021**, *9*, 1507.
[30] G. Parisi, A. Lopez, S. Narayan, *ACS Appl. Eng. Mater.* **2023**, *1*, 408.
[31] N. Thakur, A. Baji, A. S. Ranganath, *Appl. Surf. Sci.* **2018**, *433*, 1018.
[32] B. S. Lalia, S. Anand, K. K. Varanasi, R. Hashaikeh, *Langmuir* **2013**, *29*, 13081.
[33] W. Shi, M. J. Anderson, J. B. Tulkoff, B. S. Kennedy, J. B. Boreyko, *ACS Appl. Mater. Interfaces* **2018**, *10*, 11979.
[34] N. G. Kowalski, J. B. Boreyko, *Soft Matter* **2022**, *18*, 7148.
[35] L. Z. Huang, M. Y. Qi, W. Zhang, W. Y. Guo, M. G. Ma, *Compos. Part A Appl. Sci. Manuf.* **2023**, *172*, 107623.
[36] X. Ming, A. Guo, Q. Zhang, Z. Guo, F. Yu, B. Hou, Y. Wang, K. P. Homewood, X. Wang, *Carbon* **2020**, *167*, 285.
[37] J. Knapczyk-Korczak, U. Stachewicz, *Nanoscale* **2021**, *13*, 16034.
[38] A. R. O. Chin, P. Guzmán-Delgado, S. C. Sillett, J. Orozco, R. D. Kramer, L. P. Kerhoulas, Z. J. Moore, M. Reed, M. A. Zwieniecki, *Am. J. Bot.* **2022**, *109*, 564.
[39] A. M. Pornea, J. M. C. Puguan, V. G. Deonikar, H. Kim, *J. Ind. Eng. Chem.* **2020**, *82*, 211.
[40] P. K. Szewczyk, A. Gradys, S. K. Kim, L. Persano, M. Marzec, A. Kryshtal, T. Busolo, A. Toncelli, D. Pisignano, A. Bernasik, S. Kar-Narayan, P. Sajkiewicz, U. Stachewicz, *ACS Appl. Mater. Interfaces* **2020**, *12*, 13575.
[41] S. Zhang, M. Zhou, M. Liu, Z. H. Guo, H. Qu, W. Chen, S. C. Tan, *Nat. Commun.* **2023**, *14*, 3245.
[42] T. Busolo, P. K. Szewczyk, M. Nair, U. Stachewicz, S. Kar-Narayan, *ACS Appl. Mater. Interfaces* **2021**, *13*, 16876.
[43] S. Zhang, Y. Zhou, A. Libanori, Y. Deng, M. Liu, M. Zhou, H. Qu, X. Zhao, P. Zheng, Y.-L. Zhu, J. Chen, S. C. Tan, *Nat. Electron.* **2023**, *6*, 338.

[44] S. Zhang, Y. Deng, A. Libanori, Y. Zhou, J. Yang, T. Tat, L. Yang, W. Sun, P. Zheng, Y. L. Zhu, J. Chen, S. C. Tan, *Adv. Mater.* **2023**, *35*, 2207916.
[45] P. K. Szewczyk, D. P. Ura, S. Metwally, J. Knapczyk-Korczak, M. Gajek, M. M. Marzec, A. Bernasik, U. Stachewicz, *Polymers* **2019**, *11*.
[46] J. Knapczyk-Korczak, J. Zhu, D. P. Ura, P. K. Szewczyk, A. Gruszczyński, L. Benker, S. Agarwal, U. Stachewicz, *ACS Sustain. Chem. Eng.* **2021**, *9*, 180.
[47] L. Zhong, R. Zhang, J. Li, Z. Guo, H. Zeng, *Langmuir* **2018**, *34*, 15259.
[48] J. Knapczyk-Korczak, P. K. Szewczyk, D. P. Ura, K. Berent, U. Stachewicz, *RSC Adv.* **2020**, *10*, 22335.
[49] K. Yin, H. Du, X. Dong, C. Wang, J. A. Duan, J. He, *Nanoscale* **2017**, *9*, 14620.
[50] M. Ahmad, A. Nighojkar, A. Plappally, *Environ. Sci. Pollut. Res.* **2023**, *31*, 10395.
[51] A. Rajabi-Abhari, M. Soltani, K. Golovin, N. Yan, *Nano Energy* **2023**, *115*, 108752.
[52] J. Wu, L. Zhang, Y. Wang, P. Wang, *Adv. Mater. Interfaces* **2017**, *4*, 1600801.
[53] M. Du, Y. Zhao, Y. Tian, K. Li, L. Jiang, *Small* **2016**, *12*, 1000.
[54] N. G. Kowalski, W. Shi, B. S. Kennedy, J. B. Boreyko, *ACS Appl. Mater. Interfaces* **2021**, *13*, 38826.
[55] R. Labbé, C. Duprat, *Soft Matter* **2019**, *15*, 6946.
[56] S. Protiere, C. Duprat, H. A. Stone, *Soft Matter* **2013**, *9*, 271.
[57] D. Nioras, K. Ellinas, V. Constantoudis, E. Gogolides, *ACS Appl. Mater. Interfaces* **2021**, *13*, 48322.
[58] Y. Ji, W. Yang, X. Li, K. Hou, P. Du, H. Zhao, Z. Fan, B. Xu, Z. Cai, *Small* **2023**, *19*, 2304037.
[59] L. M. C. Dadios, S. M. B. Encina, G. J. D. Recalde, O. M. G. Tomampoc, A. C. Abad, *C. DLSU Research Congress* **2013**, *1*.
[60] A. D. Penwarden, *Build. Sci.* **1973**, *8*, 259.
[61] Y. Uzun, S. Demirbas, E. Kurt, *Elektron. Elektrotech.* **2014**, *20*, 35.
[62] P. Pazhamalai, V. K. Mariappan, S. Sahoo, W. Y. Kim, Y. S. Mok, S. J. Kim, *Micromachines* **2020**, *11*, 198.
[63] S. Zhang, M. Chi, J. Mo, T. Liu, Y. Liu, Q. Fu, J. Wang, B. Luo, Y. Qin, S. Wang, S. Nie, *Nat. Commun.* **2022**, *13*, 1.
[64] C. Ma, L. Chen, L. Wang, W. Tong, C. Chu, Z. Yuan, C. Lv, Q. Zheng, *Nat. Commun.* **2022**, *13*, 1.
[65] F. J. Diaz Sanchez, M. Chung, M. Waqas, V. Koutsos, S. Smith, N. Radacsi, *Nano Energy* **2022**, *98*, 107286.
[66] B. Sun, D. Chao, C. Wang, *Chem. Res. Chinese Univ.* **2022**, *38*, 1005.
[67] M. N. Uddin, F. J. Desai, M. M. Rahman, R. Asmatulu, *Nanoscale Adv.* **2020**, *2*, 4627.
[68] X. Du, Z. Zhou, Z. Zhang, L. Yao, Q. Zhang, H. Yang, *J. Adv. Ceram.* **2022**, *11*, 331.
[69] Y. Guo, Y. Li, G. Zhao, Y. Zhang, G. Pan, H. Yu, M. Zhao, G. Tang, Y. Liu, *Langmuir* **2023**, *39*, 4642.
[70] W. Fan, C. Zhang, Y. Liu, S. Wang, K. Dong, Y. Li, F. Wu, J. Liang, C. Wang, Y. Zhang, *Nano Res.* **2023**, *16*, 11612.
[71] K. G. Motora, C. M. Wu, G. M. Rani, W. T. Yen, K. S. Lin, *Renew. Energy* **2023**, *217*, 119208.
[72] H. Güçlü, H. Kasım, M. Yazici, *J. Compos. Mater.* **2023**, *57*, 409.
[73] D. Li, Y. Fan, G. Han, Z. Guo, *Chem. Eng. J.* **2021**, *404*, 126515.
[74] S. Wang, K. Shi, B. Chai, S. Qiao, Z. Huang, P. Jiang, X. Huang, *Nano Mater. Sci.* **2022**, *4*, 126.
[75] J. Knapczyk-Korczak, P. K. Szewczyk, U. Stachewicz, *RSC Adv.* **2021**, *11*, 10866.
[76] S. Wu, F. Zabihi, R. Y. Yeap, M. R. Y. Darestani, A. Bahi, Z. Wan, S. Yang, P. Servati, F. K. Ko, *ACS Nano* **2022**.
[77] G. Parisi, P. K. Szewczyk, S. Narayan, U. Stachewicz, *ACS Appl. Mater. Interfaces* **2023**, *15*, 40001.
[78] M. Khalifa, S. Peravali, S. Varsha, S. Anandhan, *JOM* **2022**, *74*, 3162.
[79] Y. Khazani, E. Rafiee, A. Samadi, *Colloids Surfaces A Physicochem. Eng. Asp.* **2023**, *675*, 132004.
[80] N. Turdakyn, Z. Bekezhankyzy, S. Araby, R. Montazami, Z. Bakenov, G. Kalimuldina, *Energy Rep.* **2023**, *10*, 628.